ACS Photonics
Article
pubs.acs.org/journal/apchd5

Lasing from Glassy Ge Quantum Dots in Crystalline Si

Martyna Grydlik,[‡] Florian Hackl, Heiko Groiss, Martin Glaser, Alma Halilovic, Thomas Fromherz, Wolfgang Jantsch, Friedrich Schäffler, and Moritz Brehm[*,‡]

Institute of Semiconductor and Solid State Physics, Johannes Kepler University Linz, Altenbergerstrasse 69, A-4040 Linz, Austria

Supporting Information

ABSTRACT: Semiconductor light-emitters compatible with standard Si integration technology (SIT) are of particular interest for overcoming limitations in the operating speed of microelectronic devices. Light sources based on group IV elements would be SIT-compatible, but suffer from the poor optoelectronic properties of bulk Si and Ge. Here we demonstrate that epitaxially grown Ge quantum dots (QDs) in a defect-free Si matrix show extraordinary optical properties if partially amorphized by Ge-ion bombardment (GIB). In contrast to conventional SiGe nanostructures, these QDs exhibit dramatically shortened carrier lifetimes and negligible thermal quenching of the photoluminescence (PL) up to room temperature. Microdisk resonators with embedded GIB-QDs exhibit threshold behavior as well as a superlinear increase of the integrated PL intensity with concomitant line width narrowing as the pump power increases. These findings demonstrate light amplification by stimulated emission in a fully SIT-compatible group IV nanosystem.

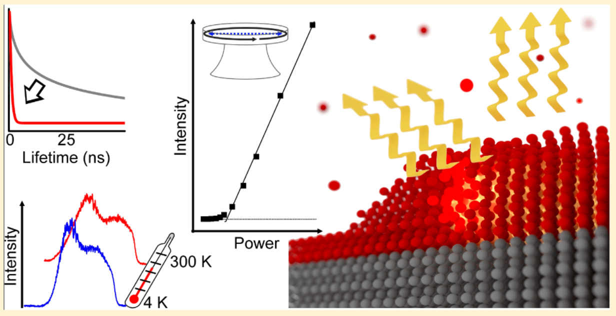

KEYWORDS: *quantum dots, photoluminescence, silicon photonics, laser, microdisks*

Silicon micro- and nanophotonics is a field of tremendous applied and basic research interest: it connects Si photonics with Si-based microelectronics and aims at the incorporation of optical functionality into integrated circuits. Widespread applications range from power electronics, and sensors all the way toward improving on-chip data communication and processing by using guided light for data transfer instead of copper wires.[1−3] The main problem arises from the poor light emission from Si and Ge, which results from the indirect bandgap of crystalline group IV materials. Recent advances in Si photonics include demonstrations of highly doped or laser-annealed Si light-emitting diodes,[4,5] an electrically pumped Ge laser,[6] group III−V QD lasers that are either grown epitaxially[7] or bonded onto Si substrates[8] and PL from strained Ge.[9−11] Most recently, a SnGe laser grown on Si was demonstrated[12] to operate up to 90 K, but shows thermal quenching by about 2 orders of magnitude between 20 and 300 K.[12]

Utilizing group IV nanostructures in Si would eliminate the growth of thick, dislocation-rich GaAs or SiGe buffer layers, necessary for some of the approaches described above. The development of crystalline Ge-QDs on Si (Ge/Si-QDs) grown by strain-driven self-organization[13−20] gave hope that quantum-confinement effects in group IV nanostructures could be used to produce high-performance optical devices. However, their optical properties never matched expectations. Because of the relatively small lattice mismatch between Si and Ge (~4%), the resulting QDs become at least in one spatial direction larger than several tens of nm. Thus, their carrier wave functions have one- or two-dimensional (1D, 2D) character rather than the zero-dimensional (0D) one aimed at. Another drawback is the spatially indirect recombination path in Ge/Si-QDs due to a type-II band alignment,[21] where only holes are confined in the Ge-QDs. Consequently, efficient room-temperature PL from crystalline Ge/Si-QDs was never observed.[14,15,18−20,22] Because of strong confinement in all three spatial dimensions as well as surface termination effects, porous silicon, and Si- and Ge-nanocrystals (Si-NCs and Ge-NCs) show significantly better optical properties at room temperature (RT).[23−28] Nevertheless, no RT continuous-wave lasing was reported so far.

In this work, we close the gap between SIT-compatible Ge/Si-QDs[29] and porous Si/Si-NCs with their superior PL properties by bombarding self-organized Ge/Si-QDs during epitaxial growth with Ge ions. This leads to partially amorphized Ge-QDs embedded in a dislocation-free Si matrix. The nucleation of strain-driven Ge/Si-QDs[13−18] occurs on a supersaturated Ge wetting layer (WL), once a critical thickness of ~4.2 monolayers (~0.6 nm) is exceeded.[30] Deposition of 0.7 nm of Ge at 500 °C leads to small hut-shaped QDs[13] with a very narrow height distribution of 1.95 ± 0.29 nm (see Supporting Information). The dot-density can be tuned between 2×10^{10} cm^{-2} (Figure 1A) and 2×10^{11} cm^{-2} (Figure 1B) by varying the Ge coverage. During Ge deposition, the sample is bombarded by positively charged Ge ions (dose: ~10^4 μm^{-2}) that are accelerated by voltages V_{GIB} of down to −2.8 kV. The high-resolution transmission electron microscopy (TEM) image in Figure 1C reveals a partly crystalline, partly

Received: November 23, 2015
Published: January 26, 2016

DOI: 10.1021/acsphotonics.5b00671
ACS Photonics 2016, 3, 298−303

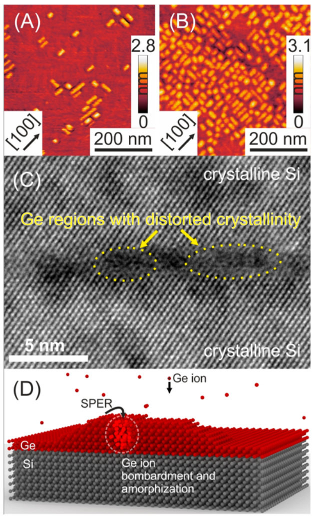

Figure 1. (A, B) Atomic force microscopy images of uncapped GIB-QDs where (A) 0.7 nm and (B) 0.84 nm of Ge were deposited at 500 °C under $V_{GIB} = -2.8$ kV. (C) High-resolution TEM image of a GIB-QD. The GIB-QD is embedded in a crystalline Si matrix and partly exhibits a glassy atomic arrangement due to the partial amorphization. (D) Ge ions impinge on the surface causing local, a few nm wide amorphization in an ellipsoidal region. During growth solid phase recrystallization (SPER) takes place reconstructing the top layers of the Ge-QD starting from still crystalline parts.

amorphized GIB-QD embedded in a crystalline Si matrix. Amorphization results in a blurring of the {111}-crystal-lattice fringes due to displaced atomic positions, in contrast to the regular atomic arrangement in the Si layer below and above the GIB-QD.

The underlying mechanism for partial amorphization is based on a collision-cascade of elliptical shape consisting of matrix atoms that become displaced by impact of either the original Ge ion or a recoil atom with an energy exceeding the displacement energy of ∼14 eV[31,32] (Figure 1D). The cascade of a single Ge ion (≲3 keV) produces one small, a few nm wide amorphous zone. During Ge deposition and ramp-down to the growth-temperature of the Si capping layer, vertical and lateral solid-phase epitaxial regrowth (SPER) takes place that leads to a recrystallization of the WL and parts of the Ge islands[33−35] (Figure 1D). This allows for partial overgrowth with a fully crystalline Si cap layer (Figure 1C). In this way, the original hut-cluster becomes divided into small crystalline Ge regions with diameters <4 nm separated by glassy Ge regions with higher energy gap.[36]

In Figure 2, we discuss the main PL features of such GIB-QDs. Figure 2A shows excitation-power (P_{exc}) dependent PL spectra, normalized to the intensity maximum of the GIB-QD-PL, as obtained at a sample temperature T_{PL} of 6 K. An increase of P_{exc} from 1.5 to 1600 μW shifts the onset of the PL from 1450 to 1250 nm, whereas the intensity-maximum of the GIB-QD-PL moves from 1560 to 1340 nm. The PL spectra were fitted using four Gaussians with maxima at (i) 1552, (ii) 1488,

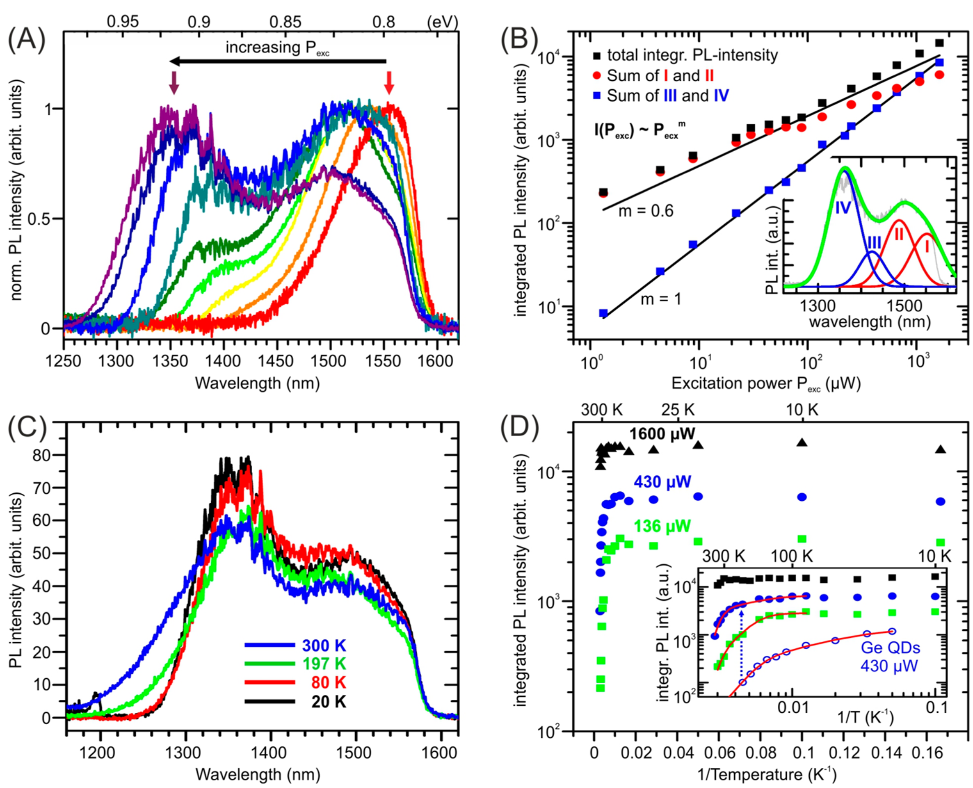

Figure 2. (A) Normalized PL spectra for increasing excitation power P_{exc}. (B) Integrated PL intensity I_{PL} vs P_{exc}. The PL spectra were fitted with four Gaussian functions (see inset). The sum of Gaussians I and II (red-circles), of Gaussians III and IV (blue squares), and the total I_{PL} (black squares) are plotted. The black solid lines represent power coefficients m of 0.6 and 1, respectively. (C) PL spectra of GIB-QDs for sample temperatures T_{PL} of 20, 80, 197, and 300 K. The spectra are to scale. (D) Full symbols: I_{PL} of the GIB-QDs vs inverse temperature for P_{exc} = 136, 430, and 1600 μW. The red curves are fits to the data. The open blue circles show I_{PL} of Ge-QDs without GIB treatment vs $1/T$ for P_{exc} = 430 μW. The blue-dashed arrow indicates the PL enhancement of the GIB-QDs as compared to crystalline Ge-QDs.

DOI: 10.1021/acsphotonics.5b00671
ACS Photonics 2016, 3, 298−303

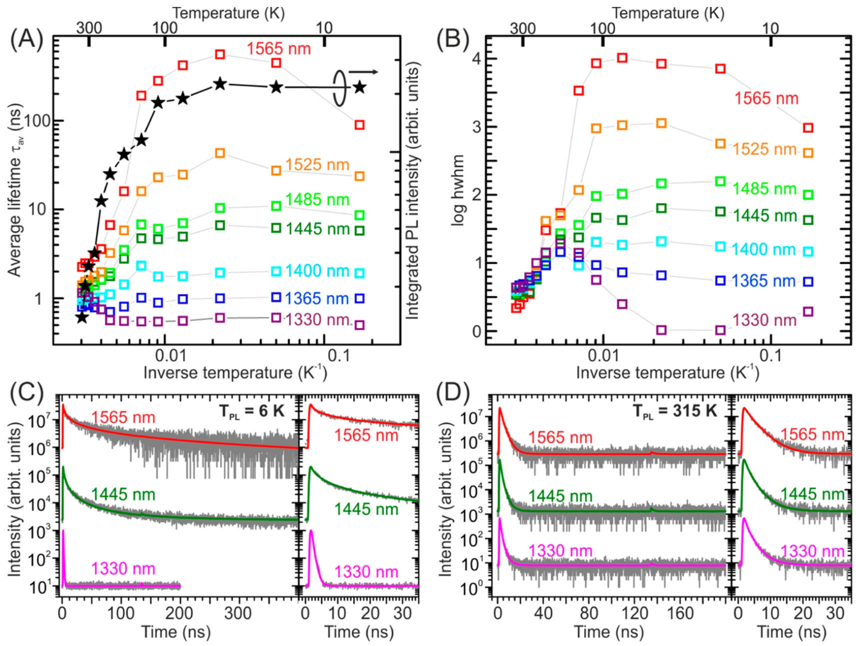

Figure 3. (A) Temperature-dependence (T_{PL}) of the average lifetimes τ_{av} for different PL-emission wavelength (open symbols) λ_{PL} = 1565 (red), 1525 (orange), 1485 (light-green), 1445 (dark-green), 1400 (light-blue), 1365 (dark-blue), and 1330 nm (violet). The corresponding integrated PL-intensity measured under pulsed excitation is plotted as full stars on the second ordinate. The gray and black lines are guides to the eye. (B) T_{PL}-dependence of the logarithmic half-width at half-maximum (hwhm) of the log-normal distribution, used to fit the λ_{PL}-dependent PL-decay spectra. (C, D) Selected time-resolved PL spectra fitted using a log-normal distribution function, red, green, and violet curve, obtained at (C) T_{PL} = 6 and (D) 315 K.

(iii) 1420, and (iv) 1352 nm and a common full-width-at-half-maximum (fwhm) of 70 nm, as shown in the inset of Figure 2B for P_{exc} = 1070 μW. In Figure 2B, the integrated PL intensity, I_{PL}, of the GIB-QDs as well as the sum of the two Gaussians with longer and shorter wavelength (i) + (ii) and (iii) + (iv), respectively, are plotted versus P_{exc}. Power laws of the form $I_{PL}(P_{exc}) \sim P_{exc}{}^{m}$ are found for the two sums, the former (i) + (ii) with $m \approx 0.6$, the latter (iii) + (iv) with $m \approx 1$. In Figure 2C, we present PL spectra (P_{exc} = 1600 μW) obtained at 20, 80, 197, and 300 K. The spectra are to scale, that is, the PL intensity hardly decreases up to 300 K. At higher T_{PL}, the onset of the GIB-QD-PL shifts to about 1200 nm. The temperature-dependent behavior of the GIB-PL for P_{exc} of 1600, 430, and 136 μW is depicted in the Arrhenius plots in Figure 2D. In the inset the data are plotted on a double logarithmic scale to emphasize the PL quenching at high T_{PL}. The solid red lines are fits to the data corresponding to activation energies E_A of ~350 meV for both P_{exc} = 136 and 430 μW. Details about the calculations of the activation energies are presented in the Supporting Information. The open blue circles in the inset of Figure 2D depict the quenching behavior (P_{exc} = 430 μW) of Ge-QDs that were grown in the same way as the GIB-QDs, but under V_{GIB} = 0 kV. Note the increase of 2 orders of magnitude of the GIB-QD PL intensity as compared to the one of the Ge-QDs at 200 K (see blue-dashed arrow in the inset of Figure 2D). For the latter, no PL is observed at RT, in agreement with previous reports in literature.[14,15,22,37−39]

We attribute the pronounced shift of the GIB-QD-PL to shorter wavelengths for increasing P_{exc} to a combination of (i) progressive filling of smaller QDs, created by the Ge ion bombardment, that, due to higher confinement energies, exhibit higher PL transition energies, (ii) state-filling within the GIB-QDs, and (iii) photoinduced band-bending effects.[22,37] In crystalline epitaxial SiGe-QDs electrons and holes are spatially separated and band filling[37] of about 100 meV is not uncommon, even for larger QDs than the ones investigated in this work, see ref 38 and the Supporting Information. In order to estimate which effect dominates, more investigations would be required, which is beyond the scope of this paper.

For very low P_{exc}, only ground states of the largest GIB-QDs are filled. For epitaxial Ge/Si-QDs, I_{PL} usually increases with P_{exc}, following a sublinear power law with $m \sim 0.6$, caused by Auger-recombination.[39] A power law with m = 1, as found here for the shorter wavelength part of the GIB-QD-PL spectrum, is usually observed in direct-gap semiconductor QDs, for example, in the III−V material system.[40] Thermal quenching with E_A ~ 60−80 meV was reported for epitaxial Ge/Si-QDs (see inset of Figure 2D),[22,39] in sharp contrast to $E_A \approx 350$ meV found here. We tentatively ascribe this high E_A to electron-occupancy of deep levels in the glassy region of GIB-QDs (see discussion of Figure 3), in analogy to deep levels caused by dangling bonds (~250−350 meV) in Si.[41]

From the discussion of Figure 2, we conclude that small GIB-QDs exhibit a different band structure scheme than the indirect and type-II band alignment of crystalline QDs. This assignment is supported by (i) the observed power law of m = 1, (ii) the high E_A in combination with the temperature stability of the GIB-QD-PL, and (iii) the fact that the k-selection rule of the indirect band gap will be softened due to Heisenberg's uncertainty principle because of strong localization of both the electron at the deep level and the holes in the GIB-QDs with diameters <~4 nm. Further support stems (iv) from the strong decrease of the average PL-decay lifetime, τ_{av}, with decreasing GIB-PL-emission wavelength λ_{PL}. Figure 3A depicts temperature- and wavelength-dependent time-decay PL spectra. For low T_{PL} < 180 K, τ_{av} is strongly wavelength-dependent: it amounts to several hundreds of ns for λ_{PL} = 1565 nm and decreases to about 600 ps for λ_{PL} = 1330 nm. For high T_{PL} >

DOI: 10.1021/acsphotonics.5b00671
ACS Photonics 2016, 3, 298−303

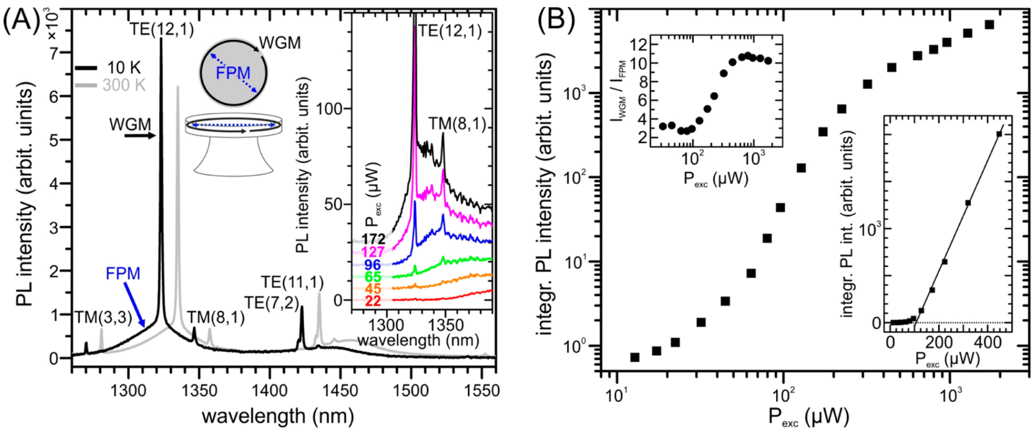

Figure 4. (A) Mode-PL-spectra from GIB-QDs in a microdisk (T_{PL} = 10 and 300 K). The inset schematically depicts the origin of the observed WGMs and FPMs. The other inset depicts the P_{exc} dependency of the PL-mode-spectrum with the emerging whispering gallery mode resonance TE(12,1). (B) Power-dependence of the integrated intensity of cavity mode TE(12,1) on a double logarithmic scale (T_{PL} = 10 K) and on a double-linear scale. The upper inset depicts the ratio I_{WGM}/I_{FPM} at 1323 nm.

300 K, τ_{av} converges to a level of about 1−2 ns, independent of the wavelength. This is consistent with the onset of thermal quenching of I_{PL} under pulsed excitation (Figure 3A, second ordinate), attributed to the increased role of nonradiative recombination processes. This is further supported by the findings of Figure 3B. There, the logarithm of the half-width at half-maximum (hwhm) of the fitted log-normal distribution functions is plotted, which gives a qualitative measure of the amount of different transition processes participating in the PL time decay.[42] A value of 0 implies a single exponential decay, higher values for hwhm imply that higher number of transition processes have to be taken into account. For T_{PL} > 250 K, the hwhm starts to converge to a level below 1, owed to nonradiative recombination processes. Figure 3C,D depicts selected time-decay spectra and fits using the log-normal distribution function for T_{PL} = 6 and 315 K and λ_{PL} of 1565, 1445, and 1330 nm. The short PL decay time of about 600 ps at 1330 nm for T_{PL} < 180 K (Figure 3A) is significantly faster than the ∼20 ns observed for Ge/Si-QD-multilayers.[19] The short τ_{av} is also consistent with the fact that the PL signal does not saturate, even in the available P_{exc} range (Figure 2B), that is, radiative recombination can compete with Auger-recombination.

To assess the potential of the GIB-QDs for lasers, we embedded them into microdisk resonators[43] of 1.8 μm diameter. The excited resonant modes are whispering-gallery modes (WGM) running around the disk's circumference and radial Fabry-Pérot modes (FPM) across the disks (see inset in Figure 4A). The former appear as sharp emission lines, and the latter as broader peaks. Figure 4A displays PL spectra of a microdisk for T_{PL} = 10 K and RT, and PL spectra for increasing P_{exc} at T_{PL} = 10 K. In the following, we will focus on the emergence of the Lorentzian-shaped transversal electrical mode TE(12,1) emitting at about 1323 nm. In Figure 4B, its integrated PL intensity, I_{WGM}, is plotted versus P_{exc} on a double-logarithmic scale, and, in the inset, on a double linear scale. The P_{exc} dependence displays threshold behavior at about 100 μW. For higher P_{exc}, I_{WGM} tends to saturate toward m = 1 (Figure 4B). Both the threshold behavior and the s-shaped I_{PL} curves are indicative of stimulated emission and can be observed up to RT. However, due to the strong filling effects of smaller GIB-QDs with higher P_{exc}, a natural threshold behavior of the cavity-mode emitting at 1323 nm is also expected (see Figure 2A). To unfold the influence of GIB-QD-filling on the threshold behavior of the TE(12,1) mode, we plotted in the inset of Figure 4B the ratio I_{WGM}/I_{FPM} versus P_{exc}. Here, I_{FPM} stands for the I_{PL} of the FPM and both I_{WGM} and I_{FPM} emit at 1323 nm, but couple to different GIB-QDs. Thus, if the threshold behavior would be caused by P_{exc}-driven filling only, we would expect I_{WGM}/I_{FPM} to remain constant versus P_{exc}. However, at the threshold, a distinct increase of I_{WGM}/I_{FPM} from 3 to about 11 is observed. Finally, we observe also line-width-narrowing (see Supporting Information) of the emission mode, which is expected for stimulated emission.

Based on these results, we expect that GIB-QDs will bridge the gap between epitaxial group IV QDs and Si-NC systems to open new paths for Si photonics based on group IV nanostructures. GIB-QDs with their separated glassy and crystalline Ge regions within an original Ge/Si-QD, are small enough to exhibit 0D-quantum confinement, similar to that of porous Si and Si-NCs. As the GIB-QDs are fully compatible with standard Si technologies, they can be monolithically integrated as electrically pumped light sources into an environment of highly complex devices together with other passive optoelectronic components based on Si.

■ METHODS

Sample Growth. Although, in this work, the samples were grown by molecular beam epitaxy (MBE) in combination with in situ low energy Ge-ion bombardment, all fabrication steps can, in principle, be performed with SIT-compatible fabrication methods. Ge quantum dots can be grown by CVD,[16] and ion implantation and annealing are standard procedures of Si device technology.

Here, the growth of GIB-QDs was carried out in a Riber SIVA45 solid-source MBE system with electron-beam evaporators for Si and Ge. We use buried-oxide SOI substrates with a SiO_2 thickness of 2 μm and a high-quality Si(001) top layer with 160 nm thickness. After ex situ sample cleaning, the natural oxide was desorbed in situ at 950 °C for 15 min. Thereafter, a 40 nm thick Si buffer layer was grown at a temperature that was ramped-down from 550 to 500 °C. A single Ge layer was grown at 500 °C with coverages of either 7 or 8.4 Å. QDs grown at such low temperatures are referred to as hut cluster or huts.[13] They are confined by 11.3° steep {105}-facets, which, due to kinetic reasons,[13] are elongated with

DOI: 10.1021/acsphotonics.5b00671
ACS Photonics 2016, 3, 298−303

a rectangular base and, thus, they resemble huts (see Figure 1A,B).

During growth, a small fraction of the evaporated Ge atoms is ionized as they pass through the electron beam of the evaporator. Those Ge ions (dose $\sim 10^4\ \mu m^{-2}$, that is, about one ion per area of $10 \times 10\ nm^2$) are then accelerated toward the substrate that is biased by an adjustable substrate bias V_{GIB} between 0 and −2.8 keV. The crystalline reference QDs were grown in the same manner but under $V_{GIB} = 0$ kV.

Finally, the GIB-QDs were embedded into a Si matrix by capping with Si. For this purpose, the substrate temperature is ramped down from the 500 °C used for Ge deposition to 350 °C for Si-cap deposition to preserve the shape and composition of the small QDs and the WL.[44] During ramp-down, the topmost part of the GIB-QDs recrystallizes laterally via solid-phase epitaxial regrowth, which then allows for overgrowth with a fully crystalline Si capping layer (see Figure 1C and, for the WL, the Supporting Information).

Optical and Structural Investigations. The surface topography was analyzed by atomic force microscopy (AFM) using a Digital Instruments Dimension 3100 AFM. To get insight into the structural properties of the GIB dots, we performed cross-sectional transmission electron microscopy using a JEOL JEM-2011 FasTEM instrument operated at 200 kV. The cross-sectional lamellae were cut by a focused ion beam using a ZEISS 1540XB CrossBeam facility.

For PL experiments, we used an excitation diode laser operated at 442 nm and a microscope objective with a numerical aperture of 0.7, which is used both for laser focusing and for collecting the PL signal from the sample. A continuous flow cryostat allows for sample cooling down to liquid He temperature. The laser spot diameter on the sample was ∼2 μm. The signal is dispersed by a grating spectrometer and recorded by a nitrogen-cooled InGaAs line detector.

For time-resolved measurements the samples were excited by a pulsed laser (wavelength of 442 nm), with a pulse width of less than 200 ps and an average optical power ranging from 7 μW to 440 μW. The time-delayed PL signal was detected by a superconducting single photon detector (SSPD) from Scontel, operated at 1.8 K. It allows single photon detection with a quantum efficiency of approximately 12% (at a wavelength λ = 1310 nm) and a counting rate larger than 70 MHz. Different emission wavelengths λ_{PL} of the PL were selected by band-pass filters with half-width at half-maximum (HWHM) of about 10 nm. Most of the decay curves of the GIB-QDs-related PL-emission show neither single- nor double-exponential behavior. They are best described by a log-normal distribution, as discussed in detail by van Driel et al.[42] The distribution of decay rates can be extracted following eq 1.

$$\sigma(\Gamma) = C \cdot \exp(-((\ln \Gamma - \ln \Gamma_{mf})/\gamma^2)) \tag{1}$$

Here, C is a normalization constant, γ is related to the hwhm of the distribution, $\Delta\Gamma$, and Γ_{mf} is the most frequent rate constant:

$$2\Delta\Gamma = 2\Gamma_{mf} \cdot \sinh(\gamma) \tag{2}$$

The average lifetime of the decay is thus calculated as follows:

$$\tau_{av} = 1/\Gamma_{mf} \cdot \exp(\Delta\Gamma^2/2) \tag{3}$$

Disk Fabrication. As a demonstrator for the incorporation of GIB-QDs into a resonant cavity, we fabricated microdisk resonators with diameters of 1.8 μm. The disk shape was written by electron-beam lithography on a LEO Supra 35 scanning electron microscope with an attached Raith Elphy plus pattern generator into a negative resist. After development, the resist acts as a mask for a reactive ion etching process in an Oxford 100 cryo-ICP etcher that is used to thin the structures down to the Si/SiO_2 interface with perpendicular sidewalls. For this process, we used the gases SF_6, He, and O_2. Hereafter, the microcavities are partially underetched by hydrofluoric acid (HF) in order to increase the mode confinement due to the larger refractive index contrast between the Si/Ge layer and the surrounding air. The carriers in the sample were optically excited, and the PL signal was detected perpendicular to the disk. The surface roughness of the disk sidewalls and the HF under-etching procedure are not fully optimized, which explains relatively low quality factors of about 1700 (see Supporting Information).

■ ASSOCIATED CONTENT

Supporting Information

The Supporting Information is available free of charge on the ACS Publications website at DOI: 10.1021/acsphotonics.5b00671.

Evaluation of the activation energies, TEM investigation of the wetting layer between the GIB-QDs, quantitative size analysis of QDs, theoretical evaluation of transition energies in crystalline QDs, estimation of the number of excitons generated per QD, and additional data concerning PL-properties of microdisk containing GIB-QDs (PDF).

■ AUTHOR INFORMATION

Corresponding Author

*E-mail: moritz.brehm@jku.at.

Author Contributions

‡These authors contributed equally (M.Gr. and M.B.).

Notes

The authors declare no competing financial interest.

■ ACKNOWLEDGMENTS

The authors gratefully acknowledge G. Bauer, K. Unterrainer, F. Bechstedt, and A. Edwards for helpful discussions, and G. Langer, O. Schmidt, and A. Rastelli for support. M.B. and H.G. gratefully acknowledge support from the Austrian Science Fund (FWF): J3328-N19 and J3317-N27. This work was also supported by the FWF-funded SFB "IRoN" via Grants F2502-N17 and F2512-N17.

■ REFERENCES

(1) Pavesi, L. Will silicon be the photonic material of the third millenium? *J. Phys.: Condens. Matter* **2003**, *15*, R1169−R1196.

(2) Soref, R. The Past, Present, and Future of Silicon Photonics. *IEEE J. Sel. Top. Quantum Electron.* **2006**, *12*, 1678−1687.

(3) Liang, D.; Bowers, J. E. Recent progress in lasers on silicon. *Nat. Photonics* **2010**, *4*, 511−517.

(4) Ng, W. L.; Lourenço, M. A.; Gwilliam, R. M.; Ledain, S.; Shao, G.; Homewood, K. P. An efficient room-temperature silicon-based light-emitting diode. *Nature* **2001**, *410*, 192−194.

(5) Sveinbjörnsson, E.Ö.; Weber, J. Room-temperature electroluminescence from dislocations in silicon. *Thin Solid Films* **1997**, *294*, 201−203.

(6) Camacho-Aguilera, R. E.; Cai, Y.; Patel, N.; Bessette, J. T.; Romagnoli, M.; Kimerling, L. C.; Michel, J. An electrically pumped germanium laser. *Opt. Express* **2012**, *20*, 11316.

DOI: 10.1021/acsphotonics.5b00671
ACS Photonics 2016, 3, 298−303

(7) Wang, T.; Liu, H.; Lee, A.; Pozzi, F.; Seeds, A. 1.3-μm InAs/GaAs quantum-dot lasers monolithically grown on Si substrates. *Opt. Express* **2011**, *19*, 11381.
(8) Liu, A. Y.; Zhang, C.; Norman, J.; Snyder, A.; Lubyshev, D.; Fastenau, J. M.; Liu, A. W. K.; Gossard, A. C.; Bowers, J. E. High performance continuous wave 1.3 μm quantum dot lasers on silicon. *Appl. Phys. Lett.* **2014**, *104*, 041104.
(9) Süess, M. J.; Geiger, R.; Minamisawa, R. A.; Schiefler, G.; Frigerio, J.; Chrastina, D.; Isella, G.; Spolenak, R.; Faist, J.; Sigg, H. Analysis of enhanced light emission from highly strained germanium microbridges. *Nat. Photonics* **2013**, *7*, 466.
(10) Sánchez-Pérez, J. R.; Boztug, C.; Chen, F.; Sudradjat, F. F.; Paskiewicz, D. M.; Jacobson, R. B.; Lagally, M. G.; Paiella, R. Direct-bandgap light-emitting germanium in tensilely strained nanomembranes. *Proc. Natl. Acad. Sci. U. S. A.* **2011**, *108*, 18893−18898.
(11) Boztug, C.; Sánchez-Pérez, J. R.; Cavallo, F.; Lagally, M. G.; Paiella, R. Strained-Germanium Nanostructures for Infrared Photonics. *ACS Nano* **2014**, *8*, 3136.
(12) Wirths, S.; Geiger, R.; von den Driesch, N.; Mussler, G.; Stoica, T.; Mantl, S.; Ikonic, Z.; Luysberg, M.; Chiussi, S.; Hartmann, J. M.; Sigg, H.; Faist, J.; Buca, D.; Grützmacher, D. Lasing in direct-bandgap GeSn alloy grown on Si. *Nat. Photonics* **2015**, *9*, 88.
(13) Mo, Y.-W.; Swartzentruber, B. S.; Lagally, M. G. Kinetic pathway in Stranski-Krastanov growth of Ge on Si(001). *Phys. Rev. Lett.* **1990**, *65*, 1020−1023.
(14) Sunamura, H.; Usami, N.; Shiraki, Y.; Fukatsu, S. Island formation during growth of Ge on Si(100): A study using photoluminescence spectroscopy. *Appl. Phys. Lett.* **1995**, *66*, 3024.
(15) Abstreiter, G.; Schittenhelm, P.; Engel, C.; Silveira, E.; Zrenner, A.; Meertens, D.; Jäger, W. Growth and characterization of self-assembled Ge-rich islands on Si. *Semicond. Sci. Technol.* **1996**, *11*, 1521.
(16) Medeiros-Ribeiro, G.; Bratkovski, A. M.; Kamins, T. I.; Ohlberg, D. A. A.; Williams, R. S. Shape Transition of Germanium Nanocrystals on a Silicon (001) Surface from Pyramids to Domes. *Science* **1998**, *279*, 353−355.
(17) Floro, J. A.; Lucadamo, G. A.; Chason, E.; Freund, L. B.; Sinclair, M.; Twesten, R. D.; Hwang, R. Q. SiGe island shape transitions induced by elastic repulsion. *Phys. Rev. Lett.* **1998**, *80*, 4717−4720.
(18) Schmidt, O. G.; Lange, C.; Eberl, K. Photoluminescence study of the initial stages of island formation for Ge pyramids/domes and hut clusters on Si (001). *Appl. Phys. Lett.* **1999**, *75*, 1905−1907.
(19) Lockwood, D. J.; Tsybeskov, L. Fast light-emitting silicon-germanium nanostructures for optical interconnects. *Opt. Quantum Electron.* **2012**, *44*, 505−512.
(20) Lee, E.-K.; Lockwood, D. J.; Baribeau, J.-M.; Bratkovsky, A. M.; Kamins, T. I.; Tsybeskov, L. Photoluminescence dynamics and Auger fountain in three-dimensional Si/SiGe multilayer nanostructures. *Phys. Rev. B: Condens. Matter Mater. Phys.* **2009**, *79*, 233307.
(21) Thewalt, M. L. W.; Harrison, D. A.; Reinhart, C. F.; Wolk, J. A. Type II Band Alignment in $Si_{1-x}Ge_x$/Si(001) Quantum Wells: The Ubiquitous Type I Luminescence Results from Band Bending. *Phys. Rev. Lett.* **1997**, *79*, 269.
(22) Dashiell, M. W.; Denker, U.; Schmidt, O. G. Photoluminescence investigation of phononless radiative recombination and thermal-stability of germanium hut clusters on silicon(001). *Appl. Phys. Lett.* **2001**, *79*, 2261.
(23) Cullis, A. G.; Canham, L. T.; Calcott, P. D. J. The structural and luminescence properties of porous silicon. *J. Appl. Phys.* **1997**, *82*, 909.
(24) Pavesi, L.; Dal Negro, L.; Mazzoleni, C.; Franzò, G.; Priolo, F. Optical gain in silicon nanocrystals. *Nature* **2000**, *408*, 440.
(25) Timmerman, D.; Valenta, J.; Dohnalova, K.; de Boer, W. D. A. M.; Gregorkiewicz, T. Step-like enhancement of luminescence quantum yield of silicon nanocrystals. *Nat. Nanotechnol.* **2011**, *6*, 710−713.
(26) Dohnalová, K.; Gregorkiewicz, T.; Kůsová, K. Silicon quantum dots: surface matters. *J. Phys.: Condens. Matter* **2014**, *26*, 173201.
(27) Saeed, S.; Buters, F.; Dohnalova, K.; Wosinski, L.; Gregorkiewicz, T. Structural and optical characterization of self-assembled Ge nanocrystal layers grown by plasma-enhanced chemical vapor deposition. *Nanotechnology* **2014**, *25*, 405705.
(28) Saeed, S.; de Weerd, C.; Stallinga, P.; Spoor, F. C. M.; Houtepen, A. J.; Siebbeles, L. D. A.; Gregorkiewicz, T. Carrier multiplication in germanium nanocrystals. *Light: Sci. Appl.* **2015**, *4*, e251.
(29) Hrauda, N.; Zhang, J.; Wintersberger, E.; Etzelstorfer, T.; Mandl, B.; Stangl, J.; Carbone, D.; Holý, V.; Jovanović, V.; Biasotto, C.; Nanver, L. K.; Moers, J.; Grützmacher, D.; Bauer, G. X-ray Nanodiffraction on a Single SiGe Quantum Dot inside a Functioning Field-Effect Transistor. *Nano Lett.* **2011**, *11*, 2875.
(30) Brehm, M.; Montalenti, F.; Grydlik, M.; Vastola, G.; Lichtenberger, H.; Hrauda, N.; Beck, M. J.; Fromherz, T.; Schäffler, F.; Miglio, L.; Bauer, G. Key role of the wetting layer in revealing the hidden path of Ge/Si(001) Stranski-Krastanow growth onset. *Phys. Rev. B: Condens. Matter Mater. Phys.* **2009**, *80*, 205321.
(31) Averback, R. S.; de la Rubia, T. D. Displacement damage in irradiated metals and semiconductors. *Solid State Phys.* **1997**, *51*, 281−402.
(32) Carter, G.; Grant, W. A. *Ion Implantation of Semiconductors*; London Edward Arnold Ltd., 1976; pp 1−214.
(33) Williams, J. S. Solid-phase epitaxial regrowth phenomena in silicon. *Nucl. Instrum. Methods Phys. Res.* **1983**, *209*, 219−228.
(34) Spaepen, F. Structural model for interface between amorphous and crystalline Si or Ge. *Acta Metall.* **1978**, *26*, 1167−1177.
(35) Williams, J. S. Solid phase recrystallization processes in silicon. *Surface Modification and Alloying by Laser, Ion, and Electron Beams*; Poate, J. M., Foti, G., Jacobson, D. C., Eds.; Plenum Press: New York, 1983; Chapter 5, pp 133−159.
(36) Tauc, J.; Grigorovici, R.; Vancu, A. Optical Properties and Electronic Structure of Amorphous Germanium. *Phys. Status Solidi B* **1966**, *15*, 627−637.
(37) Wan, J.; Jin, G. L.; Jiang, Z. M.; Luo, Y. H.; Liu, J. L.; Wang, K. L. Band alignments and photon-induced carrier transfer from wetting layers to Ge islands grown on Si(001). *Appl. Phys. Lett.* **2001**, *78*, 1763.
(38) Brehm, M.; Grydlik, M.; Hackl, F.; Lausecker, E.; Fromherz, T.; Bauer, G. Excitation Intensity Driven PL Shifts of SiGe Islands on Patterned and Planar Si(001) Substrates: Evidence for Ge-rich Dots in Islands. *Nanoscale Res. Lett.* **2010**, *5*, 1868−1872.
(39) Tsybeskov, L.; Lockwood, D. J. Silicon-Germanium Nanostructures for Light Emitters and On-Chip Optical Interconnects. *Proc. IEEE* **2009**, *97*, 1284.
(40) Le Ru, E. C.; Fack, J.; Murray, R. Temperature and excitation density dependence of the photoluminescence from annealed InAs/GaAs quantum dots. *Phys. Rev. B: Condens. Matter Mater. Phys.* **2003**, *67*, 245318.
(41) Edwards, A. H. *Phys. Rev. B: Condens. Matter Mater. Phys.* **1991**, *44*, 1832. Edwards, A. H. Interaction of H and H_2 with the silicon dangling orbital at the (111) Si/SiO_2 interface. *Phys. Rev. B: Condens. Matter Mater. Phys.* **1991**, *44*, 1832.
(42) van Driel, A.; Nikolaev, I.; Vergeer, P.; Lodahl, P.; Vanmaekelbergh, D.; Vos, W. Statistical analysis of time-resolved emission from ensembles of semiconductor quantum dots: Interpretation of exponential decay models. *Phys. Rev. B: Condens. Matter Mater. Phys.* **2007**, *75*, 035329.
(43) Xia, J. S.; Nemoto, K.; Ikegami, Y.; Shiraki, Y. Silicon-based light emitters fabricated by embedding Ge self-assembled quantum dots in microdisks. *Appl. Phys. Lett.* **2007**, *91*, 011104.
(44) Brehm, M.; Grydlik, M.; Groiss, H.; Hackl, F.; Schäffler, F.; Fromherz, T.; Bauer, G. The influence of a Si cap on self-organized SiGe islands and the underlying wetting layer. *J. Appl. Phys.* **2011**, *109*, 123505.

DOI: 10.1021/acsphotonics.5b00671
ACS Photonics 2016, 3, 298−303